Emission- and fluorescence-spectroscopic investigation of a glow discharge plasma: Absolute number density of radiative and nonradiative atoms in the negative glow

Y. Takubo, T. Sato, N. Asaoka, K. Kusaka, T. Akiyama, K. Muroo, and M. Yamamoto
Department of Applied Physics, Tokyo University of Agriculture and Technology, Koganei, Tokyo 184-8588, Japan
(Received 6 February 2007; revised manuscript received 3 October 2007; published 15 January 2008)

The excited-state atom densities in the negative glow of a direct-current glow discharge are derived from the spectral-line intensity of radiative atoms and the resonance-fluorescence photon flux of nonradiative atoms. The discharge is operated in a helium-argon gas mixture (molar fraction ratio 91:9; total gas pressure 5 Torr) at a dc current of 0.7–1.2 mA. The observations are made in the region of the maximum luminance in the cathode region, where high-energy electrons accelerated in the cathode fall are injected into the negative glow. The emission intensities of the He I, He II, Ar I, and Ar II spectral lines are measured with a calibrated tungsten ribbon lamp as an absolute spectral-radiance standard. Fluorescence photons scattered by helium and argon atoms in the metastable state and argon atoms in the resonance state are detected by the laser-induced fluorescence (LIF) method with the Rayleigh scattering of nitrogen molecules as an absolute standard of scattering cross section. The laser absorption method is incorporated to confirm the result of the LIF measurement. Excitation energies of the measured spectral lines range from 11.6 (Ar I) to 75.6 eV (He II), where the excitation energy is measured from the ground state of the neutral atom on the assumption that, in the plasma of this study, both the neutral and the ionic lines are excited by electron impact in a single-step process from the ground state of the corresponding neutral atoms. Experimental evidence is shown for the validity of this assumption.

DOI: 10.1103/PhysRevE.77.016405 PACS number(s): 52.70.−m, 52.80.−s

I. INTRODUCTION

A direct-current glow discharge is characterized by the presence of a strong electric field localized in the cathode fall, which leads to a highly nonequilibrium electron energy distribution function (EEDF) in the regions of cathode fall and negative glow. The EEDF is one of the fundamental quantities that governs the physical processes in the discharge. Recent progress achieved in simulations of electron kinetics and modeling of gas discharges has revealed the nature of various types of plasmas [1–7]. Advanced simulation techniques can lead to improved agreement between theoretical predictions and experimental observations for the EEDF in the cathode region.

The nonequilibrium EEDF in low-current, direct-current discharges has been the subject of extensive study. Vrhovac *et al.* investigated the discharge in argon and nitrogen using a retarding potential energy analyzer [8,9]. For the discharge in nitrogen under the condition of relatively high E/N (the ratio of the electric field to the gas number density), they obtained good agreement between the measured EEDF and the Monte Carlo simulation by an exact treatment of the effects that modify the EEDF in the process of electron sampling [9]. Hannemann *et al.* [10] analyzed the behavior of electrons in the cathode region of a H_2-Ar-N_2 discharges by solving the space-dependent Boltzmann equation. They compared the result of model calculations with the experimental result of Langmuir-probe measurements performed in the negative glow and the Faraday dark space. Lawler *et al.* determined the density and temperature of cold (low-energy) electrons in the negative glow of a helium discharge by laser-induced fluorescence (LIF) and absorption spectroscopy [11,12]. The EEDF of hot electrons was obtained by the Monte Carlo simulation technique. Results from the experiments and simulations were combined to study the power balance of the low-energy electrons. They measured the spatial distribution of the absolute density of metastable atoms using LIF and absorption spectroscopy. Arslanbekov and Kudryavtsev analyzed the energy balance of the bulk electrons in the negative glow of a helium discharge by using a model that enabled the electron temperature to be predicted [13]. They computed the EEDF for slow electrons from a kinetic equation. Bogaerts *et al.* measured the three-dimensional density profile of metastable atoms in an argon glow discharge and compared the result with a mathematical model [14]. Using an extensive collisional and raditative model of the argon glow discharge, Bogaerts *et al.* obtained the spatially resolved absolute density distribution of radiative and nonradiative atoms for a number of excited states [15–17]. Baguer *et al.* calculated the argon metastable population in a hollow cathode discharge and compared it with a laser absorption measurement [18].

For continued progress in plasma modeling and better insight into physical processes, the fidelity of mathematical modeling needs to be confirmed by experiment. Electric probes and retarding potential analyzers give information about the EEDF by directly sampling plasma electrons, but these methods are intrusive to plasmas. While optical diagnosis does not disturb plasmas, the spectral-line intensity of the bound-bound transition is not directly connected to the EEDF, but is given by an integral over the EEDF multiplied by an excitation function [19–21]. The excitation function is not simply connected to a cross section but is obtained through collisional and radiative balancing between the excited states [22]. Therefore, the accuracy of the EEDF obtained from spectroscopic diagnosis depends both on the reliability of the plasma model and on the accuracy of the atomic cross sections. It is recognized that experimental verification of mathematical simulations by spectroscopic diag-

nosis requires starting with accumulation of reliable and comprehensive data for as many atomic transitions as possible. For quantitative discussions both the theoretical and the experimental quantities need to be placed on an absolute scale.

The principal purpose of the present study is to provide spectroscopic data obtained from absolute intensity measurements, which enable direct comparison of the experimental results with theoretical simulations. In this work we measure emission, absorption, and fluorescence signals of a direct-current glow discharge at the point of maximum luminance in the cathode region, where high-energy electrons accelerated in the cathode fall are injected into the negative glow. The discharge is operated in a mixture of helium and argon. The rate coefficients for argon measured by Takubo *et al.* in previous work [23] are used to analyze the relaxation process in the excited levels.

II. THEORETICAL BACKGROUND

For an optically thin plasma the density of excited atoms is related to the emission intensity of a spectral line by the following expression:

$$\epsilon = \frac{h\nu_{21}}{4\pi} A_{21} N_2, \tag{1}$$

where the emission intensity ϵ is defined as the radiant power of the spectral line emitted from a unit volume of the plasma into a unit solid angle. The quantities $h\nu_{21}$ and A_{21} are, respectively, the photon energy and the spontaneous emission coefficient for the radiative transition from the excited state 2 to the lower state 1, and N_2 is the density of radiative atoms in the excited state 2. The above expression is based on the assumption that the plasma emission is isotropic and unpolarized. (See Sec. IV B for the validity of this assumption.) The radiance of the plasma is given by the emission intensity integrated along the optical path. The radiant flux received by a detector, I, is given by

$$I = \epsilon \Phi \Delta V_r \Delta\Omega, \tag{2}$$

where ΔV_r is the volume of the plasma observed with an optical system subtending a solid angle $\Delta\Omega$ with the plasma, and Φ is the transmission coefficient of the optical system. For an inhomogeneous plasma, the spatially resolved emission intensity can be obtained from the observed spatial distribution of the radiance by the Abel inversion, provided that the plasma is optically thin and axially symmetric.

Nonradiative atoms are detected by the resonant LIF method. In this method the atomic density is related to the flux of photons scattered by the atoms. Assume that an atom in an initial state 1 scatters a photon of the laser radiation field, which has an optical frequency in resonance with the transition between the initial state 1 and the intermediate state 2 of the scattering atom. After scattering the atom is left in a final state 3 by emitting a fluorescence photon of energy $h\nu_{23}$ corresponding to the energy difference between the states 2 and 3. The density of atoms in the initial state, N_1, is related to the number of fluorescence photons, F_f, received by the detector for each pulse of the excitation laser by the following expression:

$$F_f = C \frac{F_e}{a\delta} N_1 \Phi \Delta V_f \Delta\Omega, \tag{3}$$

where C is a coefficient given in terms of the differential cross section for resonance scattering, F_e is the number of photons per each pulse of the excitation laser, and a and δ are the cross section and the spectral bandwidth of the laser beam, respectively. The broadband and steady-state excitation conditions are assumed to be satisfied for the spectral bandwidth and the duration of the laser pulse. The volume of the plasma excited by the laser and monitored by the optical system is represented by ΔV_f. The transmission coefficient Φ and the solid angle $\Delta\Omega$ are the same for both the emission and the fluorescence experiments.

The theoretical expression for the differential cross section is found in the literature [24–26]. It is given in terms of the quantities $\hat{\mathbf{e}}_e \cdot \mathbf{D}_e$ and $\hat{\mathbf{e}}_f \cdot \mathbf{D}_f$, where the unit vectors $\hat{\mathbf{e}}_e$ and $\hat{\mathbf{e}}_f$ specify the polarization state of the excitation and fluorescence photons, respectively. The dipole matrix element $\mathbf{D}_e$ for the excitation transition between the initial state 1 and the intermediate state 2 and the matrix element $\mathbf{D}_f$ for the fluorescence transition between the intermediate state 2 and the final state 3 can be derived from the experimental atomic transition probabilities. The scattering cross section is also dependent on the relaxation coefficient for the intermediate state, Γ_2, which is given in terms of the radiative and quenching transition rates for the intermediate state, and in terms of the rate of dephasing collisions for this state causing fluorescence depolarization.

In accordance with the experimental setup, we assume that the fluorescence photons are detected in a direction perpendicular to the incident plane of the laser beam, and that the laser light is linearly polarized in the incident plane. In view of the possibility of fluorescence depolarization due to dephasing collisions, we measure the polarization components in directions parallel and perpendicular to the incident-light polarization [27,28]. Actually, deviation of the measured polarization ratio from the theoretical value predicted in the absence of depolarizing collisions could not be detected within the experimental accuracy. For the excitation and fluorescence transitions measured in this study, the ratio of the parallel to vertical components in the absence of depolarization is 1:0 for the He I $2s\ ^1S \rightarrow 3p\ ^1P^o \rightarrow 2s\ ^1S$ transition, 6:7 for the Ar I $1s_5 \rightarrow 2p_2 \rightarrow 1s_4$ transition, and 1:1 for the Ar I $1s_4 \rightarrow 3p_5 \rightarrow 1s_2$ transition. The Paschen notation is used for the neutral argon atom throughout this paper.

III. EXPERIMENTAL METHOD

A. Emission measurement

The experimental apparatus was essentially the same as that used in our previous studies [23,29,30]. The discharge plasma was generated between a pair of electrodes. The top electrode (anode) was a disk of 50 mm in diameter. The water-cooled bottom electrode (cathode) was a disk of 10 mm in diameter. It was separated from the anode by a dis-

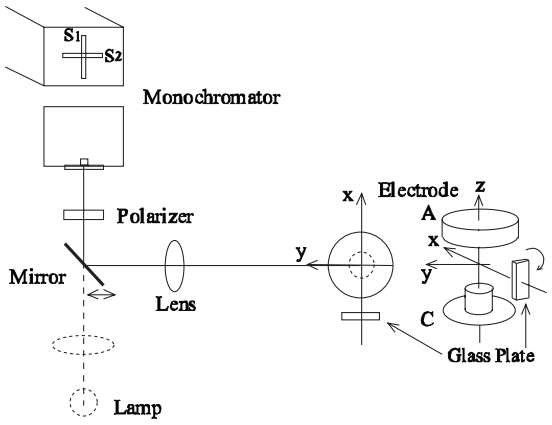

FIG. 1. Experimental setup. *A*, anode; *C*, cathode.

tance of 10 mm. Positive high voltage was applied to the anode and the cathode was grounded. A helium-argon gas mixture with a molar fraction ratio of 91:9 flowed into the discharge chamber through 37 apertures of 1 mm diameter bored in the top electrode. The total flow rate of the gas mixture was 400 cm^3/min and the total gas pressure in the discharge chamber was 5 Torr. The gas-feeding apertures were uniformly distributed over the surface of the anode disk. The calculated velocity of gas flow ejected from each of the gas-feeding apertures was about 1/10 of the thermal velocity of argon atoms. Since the region of the discharge where spectroscopic observations are made is 7.5 mm apart from the gas-feeding aperture (see below), the directional velocity of the gas flow is considered to be slower in this region. Experiments were made over a range of the discharge current from 0.7 to 1.2 mA dc. In this current region the cathode to anode voltage and the power input into the discharge was 200 V, 140 mW at 0.7 mA, 220V, 220 mW at 1.0 mA, and 225 V, 270 mW at 1.2 mA. The average value of E/N in the cathode fall estimated from the cathode to anode potential, the cathode fall length, and the gas density, was approximately 1.6 kTd [1 Townsend (Td) $=10^{-17}$ V cm^2]. The discharge had a region of bright glow between the anode and the cathode. The radiance of the plasma reached its maximum at a height 2.5 mm above the cathode surface, as shown in Sec. IV B. At this height we scanned the plasma in the horizontal direction to measure the radial distribution of the radiance. The true radial distribution of the emission intensity was derived from the measured radiance distribution by the Abel inversion.

The optical system is shown in Fig. 1. A fused silica lens of 200 mm focal length was used to form a 1:1 image of either the plasma or the tungsten ribbon lamp on the entrance slit S_1 of a grating monochromator. Three lenses of different curvature were prepared for use in different wavelength regions to minimize chromatic aberration. A tungsten ribbon lamp (Eppley Laboratory, Model EP) served as an absolute standard for the spectral radiance. The focal length of the monochromator was 1 m, and the width of both the entrance slit S_1 and the exit slit was 0.25 mm. The spectral resolution of the monochromator was 0.2 nm. A slit of 1 mm height (S_2) was placed in front of the slit S_1. A reflecting mirror put on the optical path was translated in the horizontal direction to measure the radial distribution of the plasma radiance. In the emission measurement the spatial resolution was determined by the width of the slit S_1 and the height of the slit S_2. The reflecting mirror was removed when the radiance standard lamp was measured. Optical output from the monochromator was detected with a photomultiplier tube followed by an electrometer or a photon counter. The transmission coefficient of the optical system including the monochromator was calibrated for the two independent directions of light polarization by placing a plastic polarizer between the lens and the monochromator. One of the sources of uncertainty involved in the measurement of the spectral-line radiance was imperfect reproducibility of the measured spectral-line intensity in successive experiments. In our experiment the radiance of the plasma and the standard lamp was reproducible within the error of 10% when the same measurement was repeated after rearrangement of all the components of the optical system.

B. LIF measurement

In the LIF experiment we used a nitrogen-laser-pumped dye laser as the excitation source. The laser was pulse operated at 10 Hz with a pulse duration of 3 ns. The spectral linewidth of the laser was 20–25 GHz [full width at half maximum (FWHM)], which was sufficiently larger than the width of the observed atomic spectral lines to satisfy the broadband excitation condition. The intensity of the excitation laser was kept low enough to avoid optical saturation. Referring to Fig. 1, the excitation laser beam with a cross section of 1×1 mm^2, linearly polarized along the z axis, was passed through the discharge plasma along the x axis. Fluorescence photons scattered by the plasma were detected in a direction along the y axis. The same optical system was used both for the emission and for the fluorescence experiments. The output of the photomultiplier was connected to a photon-counting system, which was gated in synchronization with the laser pulse to suppress spontaneous emission noise of the plasma.

By scanning the laser frequency in the region of the resonant excitation transition, we counted the fluorescence photons as a function of the laser frequency (excitation-scan spectrum). The fluorescence signal was superimposed by two sources of background noise. One of the noise sources was spontaneous emission radiated by the atoms in the intermediate state 2. Another source of noise was stray light due to the laser beam scattered by the optical instrument. The contribution of the spontaneous emission was compensated for by operating the discharge while interrupting the excitation laser. The contribution of stray light was compensated for by operating the laser while interrupting the discharge. The fluorescence and the noise signals were measured at a fixed laser frequency by accumulating the photon signals during the repetition of the excitation laser pulse. The LIF measurement was made on the central axis of the plasma at a height of 2.5 mm above the cathode, i.e., at the same point as the emission measurement. Polarization of fluorescence light was analyzed with the same polarizer as that used in the emission measurement.

Spatial resolution of the LIF measurement was dependent on the cross section of the laser beam and the width of the monochromator slit S_1 on which the image of the plasma was focused. Typical values in our experiment were as follows: laser beam cross section, 1×1 mm^2; slit width, $\Delta x=0.25$ mm. A tilted glass plate was used to displace the laser beam in the interelectrode region as shown in Fig. 1. Nonradiative species detected by the LIF spectroscopy have a longer lifetime than radiative species. Due to the gas flow in the discharge region, the nonradiative atoms are forced to move a finite distance before these atoms are detected or quenched. Among the nonradiative species measured in this work, the Ar $1s_5$ metastable atom quenched by low-energy electrons has a quenching rate of $K=(5.9\pm0.8)\times10^4$ s^{-1} at a discharge current of 0.7 mA [23]. From the quenching rate and the gas-flow velocity we estimate that, besides the spatial resolution mentioned above, the LIF detection has a maximum positional uncertainty of 0.6 mm if the directional velocity of gas flow ejected from the gas-feeding aperture is assumed to continue in the interelectrode region. Other atoms of nonradiative species measured in this work have a shorter lifetime than the Ar $1s_5$ atom (see Sec. V C).

For the calibration of the absolute sensitivity of the fluorescence detection system, we introduced nitrogen gas into the discharge chamber to measure Rayleigh scattering of nitrogen molecules. The procedure of calibration has been described previously [29]. We refer to Ref. [31] for the scattering cross section of the nitrogen molecule. In the fluorescence measurement, fluctuations of the laser pulse energy were within 25%. Another source of errors in the LIF measurement were statistical fluctuations of fluorescence photons.

IV. DENSITY OF EXCITED ATOMS

A. Gas temperature

To determine the temperature of gas atoms in the discharge plasma we measured Doppler broadening of the He I emission line at 501.6nm with a Fabry-Pérot interferometer (Burleigh Instruments, R-100). The measured profile of the He I line had a total width of 4.8 GHz with an instrumental width of 1.0 GHz (FWHM). Under the experimental condition of the present work, the observed line is estimated to have a pressure broadening of 0.2 GHz [12]. By the deconvolution of instrumental and pressure widths, we obtained the true Doppler width equivalent to the gas temperature of 360 K. Broadening associated with molecular dissociation [32] was not taken into consideration because no band spectra of the He_2 molecule were observed in the region of 410–480 nm. Stark broadening due to electron impact and the quasistatic ion field was estimated to be two orders of magnitude smaller than the measured linewidth [33–35]. Broadening associated with radiative and nonradiative decay was also smaller than the measured width by two orders of magnitude.

B. Emission intensity and the density of radiative atoms

Figure 2 shows the spatial distribution of the spectral-line radiance measured by scanning the plasma in the vertical direction along the central axis of the plasma. The slit S_2 shown in Fig. 1 was displaced in the vertical direction to scan the plasma. The discharge current was 1 mA. In this figure the horizontal axis is the height from the cathode surface. All the lines attain the maximum of radiance at 2.5 mm above the cathode surface. The radiance falls both in the cathode fall region and in the Faraday dark space. The spatial dependence of the spectral-line intensity in the close vicinity of the cathode surface, which has been investigated by previous workers [15,36], could not be measured in our study because of insufficient spatial resolution limited by the 1 mm height of the slit S_2.

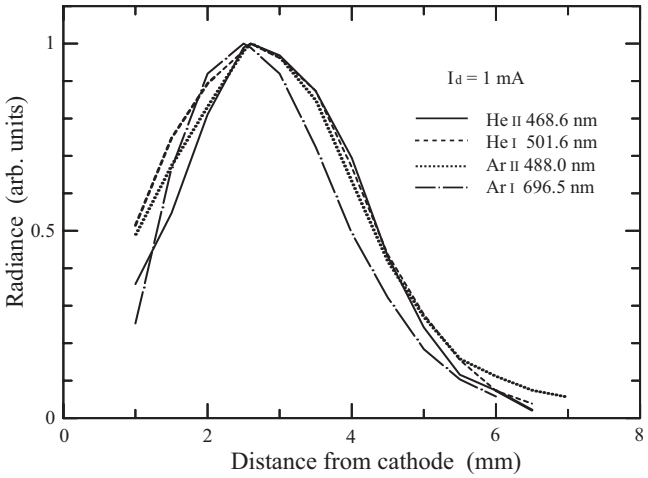

FIG. 2. Axial distribution of emission-line intensity.

Figure 3 shows the horizontal distribution of the spectral-line radiance measured at the height of 2.5 mm above the cathode. In this figure the horizontal axis is the distance from the central axis along the x axis (Fig. 1). The normalized spatial distribution of the radiance had the same profile for all the spectral lines within the experimental accuracy despite the difference in the excitation energy of these lines (13.3–75.6 eV). The normalized spatial distribution did not change in the region of the discharge current between 0.7 and 1.2 mA. Uncertainty involved in the measured spectral-

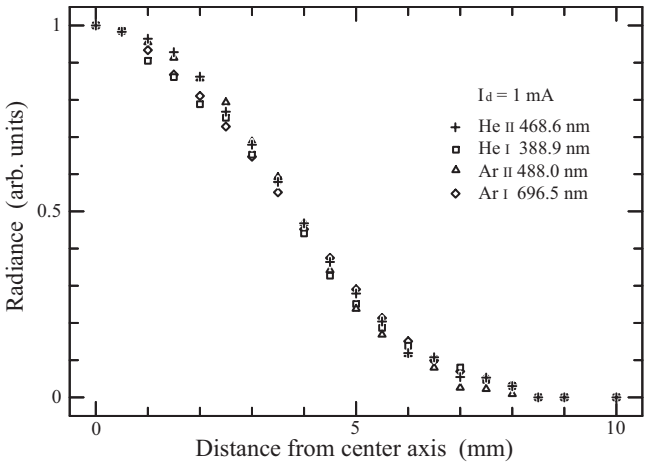

FIG. 3. Horizontal distribution of emission-line intensity.

TABLE I. Emission intensity and excited-state density of radiative species. I_d is the discharge current.

				I_d (mA)					
				0.7	1.0	1.2	0.7	1.0	1.2
Species	Wavelength (nm)	Excited level	Energy (eV)	Emission intensity (W/str cm^3)			Number density (cm^{-3})		
He II	468.6	$4f\ ^2F^o$ etc.	75.6	4.1×10^{-9}	6.4×10^{-9}	1.0×10^{-8}	8.4×10^{2}	1.3×10^{3}	2.1×10^{3}
Ar II	385.1	$4p\ ^4S^o_{3/2}$	35.7	2.3×10^{-8}	2.9×10^{-8}	3.5×10^{-8}	1.2×10^{4}	1.5×10^{4}	1.8×10^{4}
Ar II	442.6	$4p\ ^4D^o_{5/2}$	35.3	4.4×10^{-8}	6.3×10^{-8}	7.5×10^{-8}	1.5×10^{4}	2.1×10^{4}	2.5×10^{4}
Ar II	457.9	$4p\ ^2S^o_{1/2}$	35.7	5.2×10^{-8}	6.7×10^{-8}	8.5×10^{-8}	1.8×10^{4}	2.4×10^{4}	3.0×10^{4}
Ar II	465.8	$4p\ ^2P^o_{1/2}$	35.6	6.3×10^{-8}	8.4×10^{-8}	1.0×10^{-7}	2.3×10^{4}	3.1×10^{4}	3.7×10^{4}
Ar II	476.5	$4p\ ^2P^o_{3/2}$	35.6	1.1×10^{-7}	1.5×10^{-7}	1.9×10^{-7}	5.6×10^{4}	7.7×10^{4}	1.0×10^{5}
Ar II	480.6	$4p\ ^4P^o_{5/2}$	34.9	4.4×10^{-8}	5.7×10^{-8}	6.9×10^{-8}	1.7×10^{4}	2.2×10^{4}	2.7×10^{4}
Ar II	488.0	$4p\ ^2D^o_{5/2}$	35.4	5.4×10^{-8}	7.6×10^{-8}	9.6×10^{-8}	2.1×10^{4}	3.0×10^{4}	3.8×10^{4}
Ar II	496.5	$4p\ ^2D^o_{3/2}$	35.5	2.5×10^{-8}	3.5×10^{-8}	4.3×10^{-8}	2.2×10^{4}	3.1×10^{4}	3.9×10^{4}
He I	294.5	$5p\ ^3P^o$	24.0	5.4×10^{-8}	7.1×10^{-8}	7.9×10^{-8}	3.4×10^{5}	4.5×10^{5}	5.0×10^{5}
He I	318.8	$4p\ ^3P^o$	23.7	4.5×10^{-7}	5.9×10^{-7}	6.4×10^{-7}	1.8×10^{6}	2.4×10^{6}	2.6×10^{6}
He I	361.4	$5p\ ^1P^o_1$	24.0	3.2×10^{-8}	4.2×10^{-8}	4.7×10^{-8}	1.9×10^{5}	2.6×10^{5}	2.9×10^{5}
He I	388.9	$3p\ ^3P^o$	23.0	1.2×10^{-6}	1.5×10^{-6}	1.7×10^{-6}	3.1×10^{6}	3.9×10^{6}	4.4×10^{6}
He I	396.5	$4p\ ^1P^o_1$	23.7	1.1×10^{-7}	1.3×10^{-7}	1.6×10^{-7}	3.7×10^{5}	4.7×10^{5}	5.4×10^{5}
He I	447.1	$4d\ ^3D$	23.7	7.7×10^{-7}	9.7×10^{-7}	1.2×10^{-6}	8.7×10^{5}	1.1×10^{6}	1.3×10^{6}
He I	471.3	$4s\ ^3S_1$	23.6	1.7×10^{-7}	2.1×10^{-7}	2.5×10^{-7}	4.7×10^{5}	6.0×10^{5}	6.9×10^{5}
He I	492.2	$4d\ ^1D_2$	23.7	2.5×10^{-7}	3.3×10^{-7}	4.1×10^{-7}	3.8×10^{5}	5.1×10^{5}	6.3×10^{5}
He I	501.6	$3p\ ^1P^o_1$	23.1	1.6×10^{-6}	1.8×10^{-6}	2.3×10^{-6}	3.7×10^{6}	4.4×10^{6}	5.4×10^{6}
He I	504.8	$4s\ ^1S_0$	23.7	1.1×10^{-7}	1.3×10^{-7}	1.6×10^{-7}	5.5×10^{5}	6.5×10^{5}	7.5×10^{5}
He I	587.6	$3d\ ^3D$	23.1	2.1×10^{-6}	2.4×10^{-6}	3.0×10^{-6}	1.1×10^{6}	1.3×10^{6}	1.6×10^{6}
He I	667.8	$3d\ ^1D_2$	23.1	3.1×10^{-6}	4.2×10^{-6}	5.4×10^{-6}	2.1×10^{6}	2.8×10^{6}	3.5×10^{6}
He I	706.5	$3s\ ^3S_1$	22.7	1.7×10^{-6}	2.2×10^{-6}	2.5×10^{-6}	2.7×10^{6}	3.5×10^{6}	4.0×10^{6}
He I	728.1	$3s\ ^1S_0$	22.9	1.3×10^{-6}	1.8×10^{-6}	2.2×10^{-6}	3.4×10^{6}	4.6×10^{6}	5.5×10^{6}
Ar I	420.1	$3p_9$	14.5	1.3×10^{-7}	1.6×10^{-7}	1.8×10^{-7}	3.5×10^{6}	4.3×10^{6}	4.8×10^{6}
Ar I	425.9	$3p_1$	14.7	2.1×10^{-7}	2.6×10^{-7}	3.0×10^{-7}	1.5×10^{6}	1.8×10^{6}	2.0×10^{6}
Ar I	433.4	$3p_3$	14.7	1.3×10^{-7}	1.5×10^{-7}	1.8×10^{-7}	6.2×10^{6}	7.4×10^{6}	8.5×10^{6}
Ar I	433.5	$3p_2$	14.7	4.8×10^{-8}	5.7×10^{-8}	6.5×10^{-8}	3.4×10^{6}	4.1×10^{6}	4.6×10^{6}
Ar I	451.1	$3p_5$	14.6	4.8×10^{-8}	5.8×10^{-8}	6.2×10^{-8}	1.1×10^{6}	1.4×10^{6}	1.5×10^{6}
Ar I	518.8	$5s''_1$	15.3	4.2×10^{-8}	5.4×10^{-8}	6.2×10^{-8}	1.0×10^{6}	1.3×10^{6}	1.5×10^{6}
Ar I	675.3	$4d_3$	14.7	2.1×10^{-7}	2.6×10^{-7}	3.2×10^{-7}	4.4×10^{6}	5.5×10^{6}	6.7×10^{6}
Ar I	696.5	$2p_2$	13.3	5.9×10^{-7}	7.4×10^{-7}	8.8×10^{-7}	4.1×10^{6}	5.1×10^{6}	6.1×10^{6}
Ar I	714.7	$2p_4$	13.3	6.6×10^{-8}	8.6×10^{-8}	1.1×10^{-7}	4.8×10^{6}	6.2×10^{6}	7.6×10^{6}
Ar I	737.2	$4d'_4$	14.8	2.9×10^{-7}	3.6×10^{-7}	4.4×10^{-7}	6.7×10^{6}	8.5×10^{6}	1.0×10^{7}
Ar I	738.4	$2p_3$	13.3	1.1×10^{-6}	1.3×10^{-6}	1.6×10^{-6}	6.0×10^{6}	7.3×10^{6}	8.7×10^{6}
Ar I	750.4	$2p_1$	13.5	5.0×10^{-6}	6.8×10^{-6}	8.1×10^{-6}	5.3×10^{6}	7.2×10^{6}	8.7×10^{6}
Ar I	751.5	$2p_5$	13.3	2.3×10^{-6}	3.1×10^{-6}	3.5×10^{-6}	2.8×10^{6}	3.6×10^{6}	4.2×10^{6}

line radiance was 10–20 %. The source of errors were temporal fluctuations of the spectral-line radiance and imperfect reproducibility of the radiance in successive experiments. Photon statistical fluctuations in the emission measurement were small compared with intensity fluctuations.

Light emitted from the cathode region of a glow discharge may be optically polarized because beamlike electrons accelerated in the cathode fall cause alignment of the excited atoms [37]. However, the observed lines were almost depolarized; the polarization degree of the measured lines, $(I_p-I_s)/(I_p+I_s)$, was less than 4%, where I_p and I_s are the radiance of the spectral lines in the two independent polarization directions. We also assume that the plasma is an isotropic radiator, i.e., the emission intensity is the same in any direction of observation.

We measured the emission intensity of the He II, Ar II, He I, and Ar I lines. Table I shows the emission intensity ϵ derived from the radiance distribution measured on the central axis of the discharge plasma at a height of 2.5 mm above the cathode. In Table I we also show the absolute number

densities of radiative atoms obtained from the emission intensity according to Eq. (1). The data of the A coefficients were taken from Refs. [38,39].

Since we assume that all the lines are produced by an electron impact in a single-step transition from the ground state of the neutral atom, the excitation energies shown in Table I are the values measured from the ground state of the corresponding neutral atom. The single-step assumption has been made under the swarm condition in the measurement of the excitation coefficient of rare-gas ions [40]. The validity of making this assumption in our study is discussed in Sec. V B.

C. Density of nonradiative atoms

While the emission intensity is directly connected to the density of radiative atoms, the LIF signal is interpreted through the analysis of the relaxation process of the intermediate state. We therefore give an account of the excitation and relaxation processes involved in the individual fluorescence transition together with the result of nonradiative-atom density measurement.

1. He 2s ^1S metastable level

Helium atoms at the $2s\ ^1S$ metastable level were detected by exciting the $2s\ ^1S-3p\ ^1P^o$ transition at 501.6 nm and observing fluorescence photons of the inverse transition, $3p\ ^1P^o-2s\ ^1S$. The excited helium atoms are quenched by collisions with ground-state argon atoms (Penning ionization) and with ground-state helium atoms (associative ionization and excitation transfer between the $3p\ ^1P^o$ and the $3d\ ^1D$ levels). On the basis of the rate equation analysis, we calculated the relaxation coefficient for the transition $3p\ ^1P^o-2s\ ^1S$. In this calculation the rate coefficient of Penning ionization for the $3p\ ^1P^o$ level was taken from Ref. [41]. The cross section for the transfer between the $3p\ ^1P^o$ and $3d\ ^1D$ levels and the rate coefficient for quenching by He-He collisions were taken from Refs. [42,43]. Radiative transition coefficients were taken from Ref. [38]. Radiative transitions to the ground state of helium were assumed to experience imprisonment of resonance radiation (see Sec. V A).

Figure 4 shows an example of the LIF excitation-scan spectrum, which was measured without the polarizer. On account of the low intensity of the LIF signal, we removed the polarizer to avoid optical loss of the polarizer. The horizontal axis of the figure is the optical frequency measured from the center of the $2s\ ^1S-3p\ ^1P^o$ transition. In this figure we show the LIF signal superimposed on background noise of spontaneous emission. The vertical axis of the figure is the number of photons accumulated for a repetition of laser pulses of $n=1000$. The gate of the photon counting system was open for a duration of 200 ns, which was sufficiently longer than the fluorescence decay time. The polarization analysis of the LIF signal indicated that the intensity of the signal component parallel to the x axis was less than 1/10 of the component parallel to the z axis. The number density of the $2s\ ^1S$ metastable level estimated from the LIF signal is listed in Table II. The major source of error involved in the LIF measurement was statistical fluctuations of photon counts. We estimated the error by numerically fitting a trial function of Gaussian profile to the laser-scan spectrum shown in Fig. 4. The estimated error was about 40%, which was about the same as that obtained with a Lorentzian profile as the trial function.

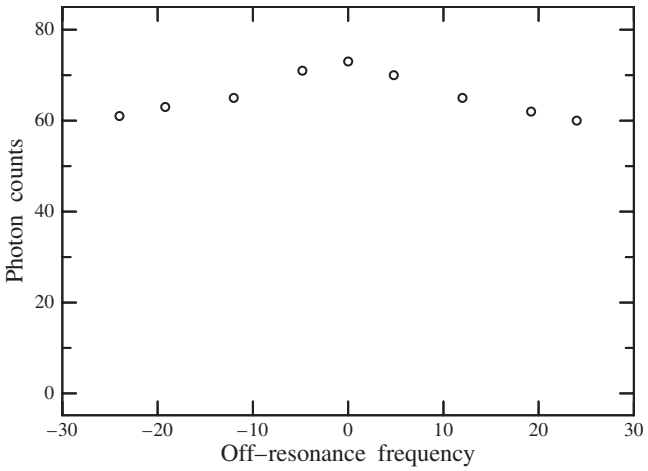

FIG. 4. LIF excitation-scan spectrum of the He $2s\ ^1S$ level. Signals involve the LIF signal and the background spontaneous emission.

2. Ar $1s_5$ metastable level

Argon atoms at the $1s_5$ metastable level were detected by exciting the $1s_5-2p_2$ transition at 696.5 nm and observing fluorescence photons of the $2p_2-1s_4$ transition at 727.3 nm. Relaxation of the intermediate $2p_2$ atoms through nonradiative transitions was investigated by observing time evolution of the fluorescence signal in the time-correlated single-photon-counting mode, which was the same as that described in Refs. [29,44] except for the excitation laser. The measured time constant for the fluorescence decay from the $2p_2$ level was 24.3 ± 3.5 ns, which agreed with the radiative lifetime of this level [39] within the experimental accuracy. We conclude, therefore, that for this level the nonradiative transition has negligible contribution to the relaxation process.

Figure 5 shows an excitation-scan spectrum of the Ar $1s_5$ metastable atom polarized along the z and x axes. The photon signals shown in the figure involve LIF photons and background noise of spontaneous emission. These photons were accumulated for a repetition of $n=3000$ pulses with a gate duration of 100 ns. Background photons detected during this repetition time were 4 counts for the polarization component parallel to the z axis and 10 counts for the component parallel to the x axis. Note that the detection sensitivity of the optical system is 2.1 times more sensitive to the x component than to the z component. The number density of the Ar $1s_5$ metastable level derived from the measured LIF signal is listed in Table II. The error due to imperfect reproducibility of the measurement was about 15% of the measured density, which was larger than statistical fluctuations of the photon count number.

The density of Ar $1s_5$ metastable atoms measured by the LIF spectroscopy was confirmed by the absorption measure-

TABLE II. Number density of nonradiative species. E, level energy; I_d, discharge current.

			I_d (mA)		
			0.7	1.0	1.2
Species	Level	E (eV)	Number density (cm^{-3})		
He I	$2s\ ^1S_0$	20.6	2.3×10^8	2.8×10^8	3.3×10^8
Ar I	$1s_5$	11.6	2.9×10^{10}	3.0×10^{10}	3.0×10^{10}
Ar I	$1s_4$	11.6	2.3×10^9	3.1×10^9	4.3×10^9

ment with a GaAlAs diode laser (Sharp Co., LT010MD) as a light source. Under the single-axial-mode operation this laser had a structure composed of seven submodes with a mode spacing of about 3 GHz and a submode bandwidth of 0.2 GHz (FWHM). The laser frequency was scanned around the $1s_5-2p_9$ transition (811.5 nm) by the temperature tuning method [45]. The laser beam of 1 mm diameter was passed in a direction parallel to the x axis at 2.5 mm above the cathode surface, and was displaced at intervals of 0.5 mm in the direction of the y axis to measure the horizontal distribution of the absorbance. A typical example of the transmission spectrum is shown in Fig. 6. The horizontal axis is the optical frequency of the central submode measured from the absorption line center. Seven absorption lines appearing in the figure correspond to the submode structure of the laser. The absorbance of the plasma was derived from the transmittance by taking into account the measured intensity distribution of the submodes. The measured spatial distribution of absorbance was converted into the radial distribution of the absorption coefficient by the Abel inversion. The density of the $1s_5$ atoms was estimated from the measured absorption coefficient by taking the calculated Doppler broadening of the argon line and the measured laser bandwidth into consideration. The density obtained from the absorption measurement was $(3.5\pm0.5)\times10^{10}$ cm^{-3} on the central axis at a discharge current of 1 mA. This result is in agreement with the value obtained by the LIF measurement within experimental accuracy.

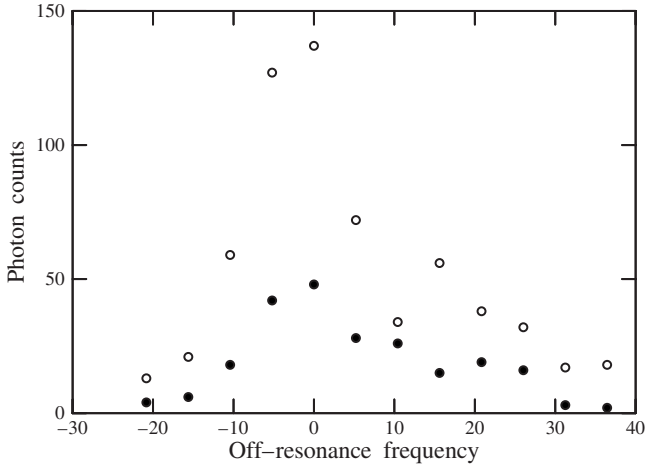

FIG. 5. LIF excitation-scan spectra of the Ar $1s_5$ level. Background emission photons are superimposed on the LIF signal. Dots, polarization component parallel to the z axis; circles, component parallel to the x axis. The optical system is 2.1 times more sensitive to the x component than to the z component.

3. Ar $1s_4$ resonance level

Radiative transitions from the Ar $1s_4$ level to the ground state experience imprisonment of resonance radiation. To detect argon atoms at the resonance level, the $1s_4-3p_5$ transition at 419.8 nm was excited and fluorescence photons of the $3p_5-1s_2$ transition at 451.1 nm were detected. The intermediate level $3p_5$ couples with the $1s$ level as well as the $2s$ and $3d$ levels through radiative transitions. Since the data for the A coefficients were available only for the $3p_i-1s_j$ transitions, we measured the lifetime of the $3p_5$ level by the time-correlated single-photon-counting method described previously. Figure 7 shows the time evolution of the fluorescence signal and the instrumental response. The decay constant for the $3p_5$ level was derived from the measured fluorescence signal by numerical deconvolution of the instrumental response. The measured fluorescence lifetime was 34.2 ± 3.5 ns. The density of the $1s_4$ resonance level obtained from the fluorescence signal is shown in Table II. Errors involved in this measurement are estimated to be 20%.

Figure 8 shows the population density of the excited levels as a function of the excitation energy. The circles are the densities of the radiative species, and the dots are those of the nonradiative species. The vertical axis is the normalized density defined as the ratio of the atomic density at each

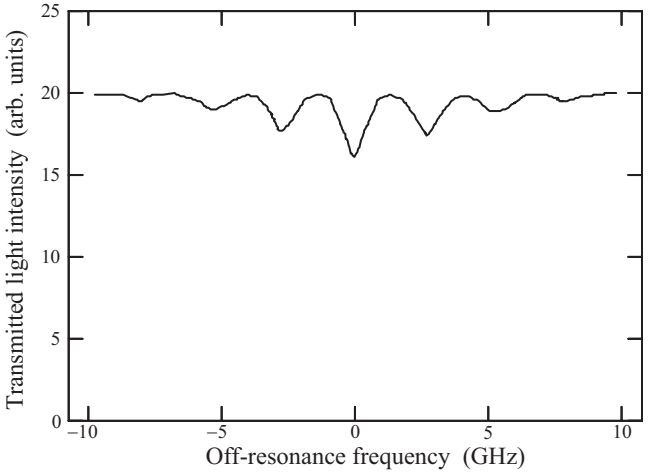

FIG. 6. Transmission spectrum of the Ar I 811.5 nm line. The horizontal axis is the laser frequency of the central submode measured from the absorption line center.

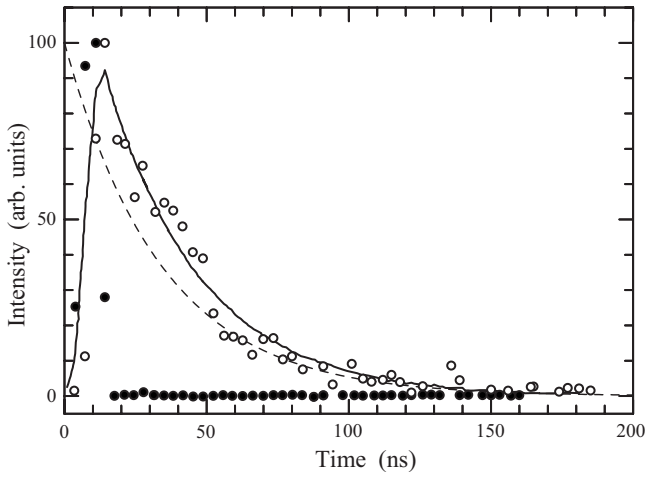

FIG. 7. Time evolution of LIF intensity (circles) and the instrumental response (dots). The solid line is fitted to the experimental points by the convolution of the instrumental response and the exponential decay curve with a 34 ns decay constant (dashed line).

substate of the excited level to the density of neutral atoms at the ground state of the corresponding atoms. The experimental points deviate from the Boltzmann distribution because detailed balance does not hold for elementary processes in a low-density, optically thin plasma.

D. Calibration of the emission signal by the LIF signal

Since on the LIF signal is superimposed the spontaneous-emission photons radiated by the atoms in the intermediate state, the emission signal can be calibrated using the LIF signal as the absolute radiation standard. Although both signals are received by the same optical system, corrections should be made for the differences in the volume of the plasma that is observed and in the duration of the signal in which the photons are generated or received. The fluorescence photons are generated from a region of the plasma that is spatially limited by the cross section of the laser beam and the width of the slit S_1. In the time domain the LIF signal is limited by the duration of the excitation laser pulse. On the other hand, the emission signal is the spectral-line intensity spatially integrated along the optical path in the direction of the y axis. In the time domain the emission signal is limited by the gate duration of the photon-counting system. These differences are corrected for by taking the experimental parameters into account.

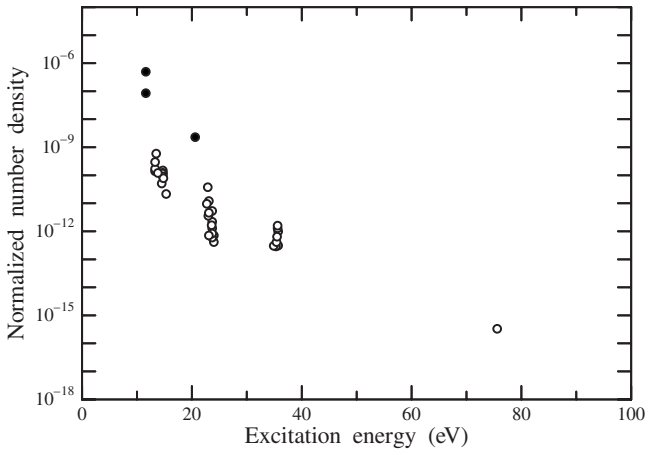

FIG. 8. Population density of the excited state as a function of excitation energy. Circles, radiative species; dots, nonradiative species. The vertical axis is the normalized density defined as the ratio of the atomic density at each substate of the excited level relative to the density of neutral atoms at the ground state of respective atoms.

We inserted the measured value of the He $2s\ ^1S$ metastable-level density into Eq. (3) to calculate the absolute intensity of the fluorescence signal. The absolute value of the exciting laser flux, F_e, was estimated from the energy of the excitation laser pulse measured with a power meter (Scientech, AC2501+AA30), together with the measured cross section of the laser beam, the pulse duration, and the laser frequency bandwidth. When the fluorescence signal evaluated by this method is used to calibrate the spontaneous emission signal, we obtained the density of the intermediate level, He I $3p\ ^1P^o$, as $(8\pm4)\times10^6$ cm^{-3} at a discharge current of 1 mA, which is in agreement with the value 4.4×10^6 cm^{-3} shown in Table I.

The same method was used to derive the density of the Ar I $2p_2$ level, the intermediate state for the measurement of fluorescence photons scattered by the Ar $1s_5$ metastable level. The result was $(9\pm3)\times10^6$ cm^{-3} at 1.2 mA, which was also in agreement with the value 6.1×10^6 cm^{-3} shown in Table I.

V. DISCUSSION

A. Optical depth

Let us verify the assumption that the plasma is optically thin for the measured emission lines. Among the spectral lines shown in Table I, transitions terminating at a nonradiative state should have the largest optical depth because of the high density populating the lower state. From the measured number densities shown in Table II and using the f values for these lines [38,39], we find that the Ar I 696.5 nm line $(2p_2-1s_5)$ has the largest optical depth. Assuming a Doppler profile for the spectral line and putting the optical-path length equal to the plasma diameter, we find that the optical depth of this line at the line center is 0.02, which is consistent with the assumption that the plasma is optically thin. Several lines of Ar I terminating at the nonradiative states, which have not been included in Table I, have a larger optical depth; for example, the 763.5 nm line $(2p_6-1s_5)$ has an optical depth of 0.2.

Among the excited levels listed in Table I, the He I $n\ ^1P$ $(n=3-5)$ levels are optically coupled to the ground state. Therefore, there is a possibility that resonance transitions from these levels experience radiation imprisonment. The radiative decay rate for the resonance level is expressed by $\gamma'=Ag$, where A is the Einstein A coefficient and g is the escape factor. The escape factor is given by the combined form of g_d and g_c, where g_d and g_c are the escape factors for Doppler and collision broadening, respectively [see Eq. (2.9)

in Ref. [46]. Using the expressions for these factors given in Ref. [47] we obtain $g_c=4.9\times10^{-4}$ and $g_d=6.3\times10^{-5}$ for the $3p\ ^1P^o$ level. This calculation is based on the measured profile of the helium emission lines and on an approximation of an infinite slab of 10 mm thickness for the geometry of the plasma. Since g_c is much larger than g_d, we can assume that $g=g_c$. Thus we obtain that $\gamma'=2.8\times10^5\ s^{-1}$. This result validates the assumption of radiation imprisonment for the resonance transition.

B. Evidence for single-step excitation

In the following description we present some of the evidence indicating that the spectral lines observed in our discharge are formed by electron impact in a single-step excitation from the ground state. Cascade processes terminating in the upper state via higher excited states are included in the single-step process.

1. Optical pumping experiment

If a cumulative excitation process exists, the dominant contribution will be made by the Ar $1s_5$ metastable level, since it has the highest density among the measured excited levels. In a recent work [23], Takubo *et al.* investigated excitation and deexcitation processes of the Ar $1s_i$ and $2p_i$ levels under the same discharge conditions as the present work. By laser pumping of the $1s_5$ metastable level to the $2p_9$ level, the density of the $1s_5$ level was depleted to less than 1/10 of the unpumped value. Observations of emission and LIF signals and the rate equation analysis indicated that pump energy absorbed by the $1s_5-2p_9$ transition was transferred to the $2p_i$ $(i\neq9)$ levels, which relaxed finally to the ground state through subsequent transitions via the $1s$ level. If cumulative transition from the $1s_5$ metastable level had significant contribution to the population of the $2p_i$ levels, the density of these levels would have been influenced by pumping up the lower level $1s_5$. The experimental result was that, with increasing density of the $2p_9$ level, the $2p_1$ density increased reaching to the maximum increment of 5% when the lower level $1s_5$ was depleted to less than 1/10. The increment of the $2p_2$ and $2p_3$ populations was less than 1%. The population increase of the $2p_i$ level is the result of competing processes between population transfer from $2p_9$ and suppression of the cumulative transition from $1s_5$. It is improbable that, for each of the $2p_i$ levels, the increment by population transfer has been balanced by the suppression of cumulative excitation. A reasonable conclusion is that cumulative transition to $2p_i$ via $1s_5$ is not a dominant process in the excitation to the $2p_i$ levels.

2. Estimation of the two-step excitation rate

Evaluation of the rate of two-step excitation from the metastable level to higher neutral levels or from the ion ground state to ionic levels needs knowledge of the EEDF in the plasma, which has been outside the scope of the present experiment. Instead, we refer to the EEDF shown in Fig. 8 of Ref. [11], which was calculated by Lawler *et al.* for a glow discharge in pure helium. Although admixture of argon into helium can affect the plasma properties considerably in our discharge, the electrode configuration, the gas pressure, the cathode to anode voltage, and the current density of Ref. [11] are similar, though not identical, to those of our discharge. We test the validity of making reference to this EEDF by comparing the emission intensity calculated according to this EEDF, ϵ_{cal}, with the intensity measured in our experiment, ϵ_{expt}. The excitation cross sections needed to calculate ϵ_{cal} are obtained from Refs. [48] (He II), [49] (Ar II), [50,51] (He I), and [52] (Ar I). The cross sections other than those for the He I lines are the apparent excitation cross sections which include the contribution of the cascade transitions. For He I lines the effect of cascade has been estimated from the measured population densities of the higher excited levels shown in Table I. Recombination of ions by radiative and collisional processes has rate coefficients that are several orders of magnitude smaller than the spontaneous emission coefficients of the measured transitions [53–56]. Quenching of the He I excited level has been discussed in Sec. IV C. The upper levels of the Ar I lines, $2p_3$ and $2p_1$, have radiative transition coefficients in the same order of magnitude as the $2p_2$ level, for which we have shown that radiative transition dominates in the decay process (Sec. IV C). We use the experimental intensity ϵ_{expt} measured at the discharge current of 0.7 mA, which is close to the current for which the calculated EEDF has been given in Ref. [11].

On the assumption of single-step excitation we obtain the calculated ratio $R_1=\epsilon_{\mathrm{cal}}/\epsilon_{\mathrm{expt}}$ shown below: R_1(He II 468.6 nm)=7.3, R_1(Ar II 488.0 nm)=8.0, R_1(Ar II 442.6 nm)=5.5, R_1(He I 388.9 nm)=3.5, R_1(He I 501.6 nm)=3.7, R_1(Ar I 738.4 nm)=7.3, and R_1(Ar I 750.4 nm)=5.8. In the energy region below the Ar I excitation threshold, we have no measured spectral lines available for the validity test. Nevertheless, we use the EEDF shown in Ref. [11] to make an approximate estimation of the two-step excitation rate by allowing for the possibility that application of this EEDF to the plasma of our study may overestimate the two-step excitation rate by a multiplication factor of the order of R_1.

The two-step excitation rate of He II and Ar II levels via the ground state of respective ions is calculated by using the cross section given in Ref. [57]. Assuming charge neutrality in the negative glow, we put the density of both helium and argon ions equal to the electron density given in Ref. [11] ignoring the possibility of overestimation. For the two-step excitation from the He metastable $2s\ ^1S$ level to the higher excited levels, we use the cross section given in Ref. [58]. Regarding the quenching rate of the excited level we follow the discussion given in Sec. IV C. For the two-step excitation from the Ar metastable level $1s_5$ to the $2p_i$ level, we adopt the apparent cross section given in Ref. [59] in the energy region $2\leq E\leq12$ eV and use the analytical expression based on the Bethe-Born approximation in the higher-energy region. The density of the metastable level has been given in Table II. From each group of the Ar II, He I, and Ar I lines shown in Table I, we select those lines which have a large ratio of the two-step cross section relative to the single-step cross section. We exclude, however, the He I lines from the $5p$ levels and the Ar I lines other than those from the $2p_i$ levels, because the two-step cross section for these transitions are not available. The calculated ratio

$R_2=\epsilon_{cal}/\epsilon_{expt}$ for two-step excitation is shown: R_2(He II 468.6 nm)$=1.0\times10^{-2}$, R_2(Ar II 496.5 nm)$=2.2\times10^{-2}$, R_2(He I 667.8 nm)$=7.3\times10^{-5}$, and R_2(Ar I 738.4 nm)$=2.0\times10^{-3}$. The calculated intensity for two-step excitation is more than two orders of magnitude smaller than the experimental intensity.

The Ar I 811.5 nm line, which has not been included in Table I, has a larger cross section for the excitation from the metastable level than from the ground state [22]. For this line we have a calculated two-step excitation rate that is 10^{-2} times smaller than the calculated rate of the single-step process. The He I $2p\ ^1P$ level has a large cross section for excitation from the $2s\ ^1S$ metastable level [58]. For this level the estimated two-step excitation rate via the metastable level is 10^{-3} times smaller than the rate of single-step excitation from the ground state. Since the density of the Ar I $1s_i(i=2-4)$ level is less than 1/10 of the $1s_5$ density (Table II and Ref. [23]), the contribution of these levels to the two-step excitation process should be small compared with that of the $1s_5$ level. It has been shown that in pure helium the two-step excitation from the He I $2s\ ^3S$ metastable level is important because of the high density ($\sim10^{12}$ cm^{-3}) of the $2s\ ^3S$ metastable atom [11]. The density of the metastable atoms in our plasma is discussed in the following section.

C. Metastable-atom density

The density of the He I $2s\ ^1S$ metastable atom measured in our experiment is by a factor of 10^{-2} lower than the value reported in Refs. [11,12] in the negative glow. The depletion of the He I $2s\ ^1S$ metastable density in our plasma is caused by quenching of the metastable level by argon atoms. The rate coefficient for Penning ionization of the helium atom by collisions with argon atoms, obtained from Ref. [41], is 3.5×10^6 s^{-1} under the experimental conditions of our study. On the other hand, spin conversion of the He I $2s\ ^1S$ metastable atom induced by electron collisions, the dominant process of quenching for this level in pure helium, is typically 7×10^4 s^{-1} [12]. Penning ionization is, therefore, responsible for the lower density of the He I $2s\ ^1S$ level in our plasma than in the pure helium plasma. The density of the He I $2s\ ^3S$ metastable atom, which has not been measured in our study, should also be reduced in our plasma. In fact, the cross section for excitation to the $2s\ ^3S$ level [50] and the cross section for Penning ionization [60] give an estimated density of the $2s\ ^3S$ level that is of the same order of magnitude as the $2s\ ^1S$ density in our plasma. The reduction of the metastable-atom density in our discharge results in corresponding decrease in the rate of two-step excitation via the metastable level.

The density of the Ar I $1s_5$ metastable level measured in our study is on the order of 10^{10} cm^{-3}, while the densities reported in the literature are on the order of 10^{10} to 10^{13} cm^{-3} depending on the discharge conditions and the position of observation. (See, for example, Ref. [14] and references therein.) The density of the Ar $2p_i$ $(i=1-4)$ levels shown in Table I and the estimated excitation rate to the $2p_i$ $(i=5-10)$ levels indicate that cascade transitions from the $2p_i$ $(i=1-10)$ levels have significant contribution to the population of the argon metastable level. The dominant decay process of metastable argon atoms is quenching collisions with slow electrons, as has been shown in previous work [23]. These results provide information for theoretical interpretation of the argon metastable density in future studies.

D. Pressure broadening

Pressure broadening of the He I 501.6 nm line reported in Ref. [61] is four times larger than the broadening reported in Ref. [12]. We have adopted the broadening coefficient reported in Ref. [12], which is consistent with the theory [62]. When the measured linewidth is corrected for the pressure broadening of Ref. [61] we have a lower gas temperature of 320 K and correspondingly higher gas density. With this correction the density of the He I $2s\ ^1S$ metastable level listed in Table II becomes 2.4×10^8 cm^{-3} at 0.7 mA, 2.9×10^8 cm^{-3} at 1.0 mA, and 3.4×10^8 cm^{-3} at 1.2 mA. The density of the Ar I $1s_5$ and $1s_4$ levels is not altered. Note that the intermediate states of fluorescence transition of the He I $2s\ ^1S$ metastable level experience quenching by collisions with helium and argon atoms, while the intermediate states for Ar I $1s_5$ and $1s_4$ decay through radiative transitions (Sec. IV C).

VI. CONCLUSION

A quantitative spectroscopic investigation has been made to measure the population density of excited atoms in a negative glow plasma generated by a dc glow discharge in a helium-argon gas mixture. The density of radiative atoms was derived from the absolute emission intensity of He I, He II, Ar I, and Ar II lines, and the density of nonradiative atoms was derived from the photon flux in LIF scattering measurements. The nonradiative levels detected were the He $2s\ ^1S$ metastable level, the Ar $1s_5$ metastable level, and the Ar $1s_4$ resonance level. The absolute densities of the excited atoms derived from the radiance of the spectral lines, the LIF photon flux, and the absorption signal were consistent with each other within the experimental accuracy. Application of the EEDF predicted in Ref. [11] for a pure helium plasma to the discharge of our study gives evidence that excited atoms of both neutral and ionic species are generated by an electron impact in a single step from the ground state of the corresponding neutral atoms. The single-step excitation is considered to dominate in the plasma of our discharge by the reduction of the density of metastable helium atoms quenched by argon atoms. This work provides spectroscopic data which enable direct comparison of the experimental results with the prediction of theoretical simulations.

ACKNOWLEDGMENTS

The authors are indebted to Y. Gomi of Japan Production Engineering Laboratory, Inc. and Dr. S. Tauchi of Hitachi, Ltd. for the technological support of this work. One of the authors (M.Y.) is grateful to Professor Y. Narahara of the University of Tsukuba for his kind advice. He is also indebted to Tokai University for the use of the library.

[1] H. C. Kim, F. Iza, S. S. Yang, M. Radmilović-Radjenović, and J. K. Lee, J. Phys. D **38**, R283 (2005).
[2] A. Bogaerts, K. de Bleecker, I. Kolev, and M. Madani, Surf. Coat. Technol. **200**, 62 (2005).
[3] J. P. Verboncoeur, Plasma Phys. Controlled Fusion **47**, A231 (2005).
[4] V. I. Kolobov and R. R. Arslanbekov, IEEE Trans. Plasma Sci. **34**, 895 (2006).
[5] R. Winkler, S. Arndt, D. Loffhagen, F. Sigeneger, and D. Uhrlandt, Contrib. Plasma Phys. **44**, 437 (2004).
[6] R. E. Robson, R. D. White, and Z. Lj. Petrović, Rev. Mod. Phys. **77**, 1303 (2005).
[7] G. G. Lister, J. E. Lawler, W. P. Lapatovich, and V. A. Godyak, Rev. Mod. Phys. **76**, 541 (2004); G. G. Lister, V. A. Sheverev, and D. Uhrlandt, J. Phys. D **35**, 2586 (2002).
[8] S. B. Vrhovac, S. B. Radovanov, Z. Lj. Petrović, and B. M. Jelenković, J. Phys. D **25**, 217 (1992).
[9] S. B. Vrhovac, V. D. Stojanović, B. M. Jelenković, and Z. Lj. Petrović, J. Appl. Phys. **90**, 5871 (2001).
[10] M. Hannemann, P. Hardt, D. Loffhagen, M. Schmidt, and R. Winkler, Plasma Sources Sci. Technol. **9**, 387 (2000).
[11] J. E. Lawler, E. A. Den Hartog, and W. N. G. Hitchon, Phys. Rev. A **43**, 4427 (1991).
[12] E. A. Den Hartog, D. A. Doughty, and J. E. Lawler, Phys. Rev. A **38**, 2471 (1988).
[13] R. R. Arslanbekov and A. A. Kudryavtsev, Phys. Rev. E **58**, 6539 (1998).
[14] A. Bogaerts, R. D. Guenard, B. W. Smith, J. D. Winefordner, W. W. Harrison, and R. Gijbels, Spectrochim. Acta, Part B **52**, 219 (1997).
[15] A. Bogaerts, J. Anal. At. Spectrom. **22**, 13 (2007).
[16] A. Bogaerts, Z. Donko, K. Kutasi, G. Bano, N. Pinhao, and M. Pinheiro, Spectrochim. Acta, Part B **55**, 1465 (2000).
[17] A. Bogaerts, R. Gijbels, and J. Vlcek, J. Appl. Phys. **84**, 121 (1998).
[18] N. Baguer, A. Bogaerts, Z. Donko, R. Gijbels, and N. Sadeghi, J. Appl. Phys. **97**, 123305 (2005).
[19] V. M. Donnelly, J. Phys. D **37**, R217 (2004).
[20] N. K. Bibinov, D. B. Kokh, N. B. Kolokolov, V. A. Kostenko, D. Meyer, I. P. Vinogradov, and K. Wiesemann, Plasma Sources Sci. Technol. **7**, 298 (1998).
[21] K. Behringer and U. Fantz, J. Phys. D **27**, 2128 (1994).
[22] J. B. Boffard, C. C. Lin, and C. A. DeJoseph, Jr., J. Phys. D **37**, R143 (2004).
[23] Y. Takubo, K. Muroo, K. Yamada, Y. Kasai, H. Kurokawa, and J. Yoseyama, Jpn. J. Appl. Phys. **42**, 5781 (2003).
[24] A. Corney, *Atomic and Laser Spectroscopy* (Clarendon Press, Oxford, 1977), Chap. 15.
[25] R. Loudon, *The Quantum Theory of Light*, 2nd ed. (Clarendon Press, Oxford, 1983), Chap. 8.
[26] A. Omont, in *Progress in Quantum Electronics*, edited by J. H. Sanders and S. Stenholm (Pergamon Press, Oxford, 1977), Vol. 5, p. 69.
[27] W. E. Baylis, in *Progress in Atomic Spectroscopy, Part B*, edited by W. Hanle and H. Kleinpoppen (Plenum Press, New York, 1979), p. 1227.
[28] C. H. Greene and R. N. Zare, Annu. Rev. Phys. Chem. **33**, 119 (1982).
[29] Y. Takubo, Y. Takasugi, and M. Yamamoto, J. Appl. Phys. **64**, 1050 (1988).
[30] M. Yamamoto, T. Sato, and Y. Takubo, J. Spectrosc. Soc. Jpn. **38**, 300 (1989).
[31] M. Sneep and W. Ubachs, J. Quant. Spectrosc. Radiat. Transf. **92**, 293 (2005).
[32] Z. Lj. Petrović, B. M. Jelenković, and A. V. Phelps, Phys. Rev. Lett. **68**, 325 (1992).
[33] H. R. Griem, *Spectral line broadening by plasmas* (Academic Press, New York, 1974).
[34] W. C. Martin and W. L. Wiese, in *Atomic, Molecular, and Optical Physics Handbook*, edited by G. W. F. Drake (AIP, Woodbury, New York, 1996), Chap. 10.
[35] N. Konjević and J. R. Roberts, J. Phys. Chem. Ref. Data **5**, 209 (1976); N. Konjević, M. S. Dimitrijević, and W. L. Wiese, *ibid.* **13**, 619 (1984).
[36] K. Rózsa, A. Gallagher, and Z. Donkó, Phys. Rev. E **52**, 913 (1995).
[37] S. A. Kazantsev and A. V. Subbotenko, J. Phys. D **20**, 741 (1987).
[38] W. L. Wiese, M. W. Smith, and B. M. Glennon, *Atomic Transition Probabilities, Vol. I*, Natl. Bur. Stand. Ref. Data Ser. Natl. Bur. Stand. (U.S.) Circ. No. 4 (U.S. GPO, Washington, D.C., 1966); W. L. Wiese, M. W. Smith, and B. M. Miles, *Atomic Transition Probabilities, Vol. II*, Natl. Bur. Stand. Ref. Data Ser. Natl. Bur. Stand. (U.S.) Circ. No. 22 (U.S. GPO, Washington, D.C., 1969).
[39] W. L. Wiese, J. W. Brault, K. Danzmann, V. Helbig, and M. Kock, Phys. Rev. A **39**, 2461 (1989).
[40] A. I. Strinić, G. N. Malović, Z. Lj. Petrović, and N. Sadeghi, Plasma Sources Sci. Technol. **13**, 333 (2004).
[41] M. H. Nayfeh, C. H. Chen, and M. G. Payne, Phys. Rev. A **14**, 1739 (1976).
[42] B. Dubreuil and A. Catherinot, Phys. Rev. A **21**, 188 (1980).
[43] A. Catherinot and B. Dubreuil, Phys. Rev. A **23**, 763 (1981).
[44] Y. Takubo, T. Okamoto, and M. Yamamoto, Jpn. J. Appl. Phys., Part 2 **24**, L263 (1985).
[45] K. Uehara, Opt. Lett. **12**, 81 (1987).
[46] P. J. Walsh, Phys. Rev. **116**, 511 (1959).
[47] T. Holstein, Phys. Rev. **83**, 1159 (1951).
[48] D. W. O. Heddle and S. M. Kay, J. Phys. B **29**, 1263 (1996).
[49] S. Tsurubuchi, J. Phys. Soc. Jpn. **66**, 3070 (1997).
[50] F. J. de Heer, R. Hoekstra, A. E. Kingston, and H. P. Summers, Nucl. Fusion Suppl. **3**, 19 (1992).
[51] T. Kato and R. K. Janev, Nucl. Fusion Suppl. **3**, 33 (1992).
[52] J. E. Chilton, J. B. Boffard, R. S. Schappe, and C. C. Lin, Phys. Rev. A **57**, 267 (1998).
[53] A. Burgess and M. J. Seaton, Mon. Not. R. Astron. Soc. **121**, 471 (1960).
[54] R. Deloche, P. Monchicourt, M. Cheret, and F. Lambert, Phys. Rev. A **13**, 1140 (1976).
[55] A. Funahashi and S. Takeda, J. Phys. Soc. Jpn. **25**, 298 (1968).
[56] M. C. M. van de Sanden, J. M. de Regt, and D. C. Schram, Phys. Rev. E **47**, 2792 (1993).
[57] I. P. Zapesochnyĭ, A. I. Imre, and Ya. N. Semenyuk, Sov. Phys. JETP **72**, 400 (1991); I. P. Zapesochnyĭ, A. I. Imre, A. I. Dashchenko, V. S. Vukstich, F. F. Danch, and V. A. Kel'man, *ibid.* **36**, 1056 (1973).
[58] F. J. de Heer, I. Bray, D. V. Fursa, F. W. Bliek, H. O. Folkerts, R. Hoekstra, and H. P. Summers, Nucl. Fusion Suppl. **6**, 7 (1995).
[59] G. A. Piech, J. B. Boffard, M. F. Gehrke, L. W. Anderson, and

C. C. Lin, Phys. Rev. Lett. **81**, 309 (1998); J. B. Boffard, G. A. Piech, M. F. Gehrke, L. W. Anderson, and C. C. Lin, Phys. Rev. A **59**, 2749 (1999).

[60] A. Hitachi, C. Davies, T. A. King, S. Kubota, and T. Doke, Phys. Rev. A **22**, 856 (1980).

[61] A. Atiola, B. C. Gibson-Wilde, A. C. Lindsay, J. L. Nicol, and I. B. Whittingham, J. Phys. B **21**, 249 (1988).

[62] D. F. T. Mullamphy, G. Peach, and I. B. Whittingham, J. Phys. B **24**, 3709 (1991).